Technical University of Denmark

DTU

On the analysis of a mixed mode bending sandwich specimen for debond fracture characterization

Quispitupa, Amilcar; Berggreen, Christian; Carlsson, Leif A.

Link back to DTU Orbit

DTU Library
Technical Information Center of Denmark

ON THE ANALYSIS OF A MIXED MODE BENDING SANDWICH SPECIMEN FOR DEBOND FRACTURE CHARACTERIZATION

A. Quispitupa[*], C. Berggreen[*1] and L. A. Carlsson[**]

[*] *Department of Mechanical Engineering, Technical University of Denmark*
Nils Koppels Allé, Building 403, DK-2800 Kgs. Lyngby, Denmark
[**] *Department of Mechanical Engineering, Florida Atlantic University*
777 Glades Road, Boca Raton, FL 33431, USA

ABSTRACT

The mixed mode bending specimen originally developed for mixed mode delamination fracture characterization of unidirectional composites has been extended to the study of debond propagation in foam cored sandwich specimens. The compliance and strain energy release rate expressions for the mixed mode bending sandwich specimen are derived based on a superposition analysis of solutions for the double cantilever beam and cracked sandwich beam specimens by applying a proper kinematic relationship for the specimen deformation combined with the loading provided by the test rig. This analysis provides also expressions for the global mode mixities. An extensive parametric analysis to improve the understanding of the influence of loading conditions, specimen geometry and mechanical properties of the face and core materials has been performed using the derived expressions and finite element analysis. The mixed mode bending compliance and energy release rate predictions were in good agreement with finite element results. Furthermore, the numerical crack surface displacement extrapolation method implemented in finite element analysis was applied to determine the local mode mixity at the tip of the debond.

Key words: Debond failure mode, sandwich structures, mixed mode bending, finite element analysis, experimental mechanics

---

[1] Corresponding author. Tel.: +45 4525 1373. Email address: cbe@mek.dtu.dk (C. Berggreen)

Nomenclature

a	crack length
b	width of the specimen
c	lever arm distance
c_m	stiffness parameters of the materials above and below the interface crack
h	characteristic distance to calculate the mode mixity at the crack tip
h_c	core thickness
h_f	face sheet thickness
k	shear correction factor
x	short distance behind the crack tip
A	extensional stiffness for a sandwich case
B	coupling stiffness for a sandwich case
C_{CSB}	compliance of the cracked sandwich beam
C_{DCB_lower}	compliance of the lower sub-beam of the double cantilever beam
C_{DCB_upper}	compliance of the upper sub-beam of the double cantilever beam
C_{DCB}	$C_{DCB\_upper} + C_{DCB\_lower}$ total compliance of the double cantilever beam
C_{MMB}	compliance of the mixed mode bending sandwich specimen
D	bending stiffness for a sandwich case
D_1	$E_f h_f^3/12$ (upper sub-beam at the debonded region)
D_2	$D-B^2/A$ (lower sub-beam at the debonded region of the sandwich specimen)
$D_{debonded}$	effective flexural stiffness of the debonded region of the cracked sandwich beam
D_{intact}	flexural stiffness of the intact region of the cracked sandwich beam
E_c	elastic modulus of the core
E_f	elastic modulus of the face sheet
G	energy release rate calculated from finite element analysis
G_{CSB}	energy release rate of the cracked sandwich beam
G_{DCB}	energy release rate of the double cantilever beam
G_f	shear modulus of the face sheet
G_{MMB}	energy release rate of the mixed mode bending sandwich specimen
G_m	shear modulus of the materials at the interface crack
G_{xz}	shear modulus of the core
G_{II}/G_I	global mixed mode ratio
K	elastic foundation modulus
$2L$	span length
P	load applied to the mixed mode bending specimen at a distance c
P_I	mode I load
P_{II}	mode II load
P_R	reaction load at the right support of the mixed mode bending specimen
α	parameter to partition the reaction load at the left support
β	parameter to partition the reaction load at the left support, or equal to $1-\alpha$
β	Dundur's parameter
ε	oscillatory index at the crack tip
η	parameter for the elastic foundation modulus
ψ	mode mixity at the crack tip
δ_c	displacement of the central part of the mixed mode bending sandwich specimen
δ_{CSB}	displacement of the cracked sandwich beam
δ_{DCB_lower}	displacement of the lower sub-beam of the double cantilever beam
δ_{DCB_upper}	displacement of the upper sub-beam of the double cantilever beam
δ_{DCB}	$\delta_{DCB\_upper} + \delta_{DCB\_lower}$ total displacement of the double cantilever beam
δ_{MMB}	displacement of the mixed mode bending sandwich specimen
δ_x	shear relative displacement of the crack flanks
δ_y	opening relative displacement of the crack flanks
Δ	displacement of the mixed mode bending specimen loaded by P_I
υ_m	Poisson's ratio

1   INTRODUCTION

Sandwich constructions are often utilized in wind turbine blades, naval and aerospace structures. Debonds between the face and core have a detrimental effect on sandwich structures since the load transfer between face and core is compromised. In the worst case scenario a debond could grow unstably with the risk of catastrophic failure of the structure. Debonds and other interfacial flaws may be introduced during manufacturing and they might grow under both static and cyclic loading during the service lifetime of the structure [1-3]. The different isotropic and orthotropic constituents of widely different material properties render the analysis of this interfacial failure mode quite complex.

Due to the bimaterial character of the face/core interface in a sandwich, the analysis of fracture must recognize the mixed mode loading and that the fracture toughness depends on the relative amount of mode I and mode II at the debond tip [4-6]. Hence, it is important to develop reliable and efficient tests methods which enable accurate measurements of the mixed mode debond toughness.

The primary objective of this paper is to establish a test principle for the study of propagation of face/core debonds under static mixed mode loading. Subsequently, the test principle will be extended to the study of crack growth during cyclic loading. Hence, it is desirable that the local mode mixity does not strongly depend on crack length.

Several tests methods have been proposed during the last two decades for static debond fracture characterization of sandwich composites. Specimens such the cracked sandwich beam (CSB) [7], double cantilever sandwich beam (DCB) [8], tilted sandwich debond specimen (TSD) [9], three point sandwich beam (TPSB) [10], single cantilever sandwich specimen (SCS), end-loaded sandwich specimen (ELSS) and the DCB subjected to uneven bending moment named DCB-UBM [11] were proposed (Fig. 1). All sandwich specimens have an artificial debond at the face/core interface. Furthermore, all specimens, except the DCB-UBM (with fixed mode mixity), the mode mixity changes as the debond length increases.
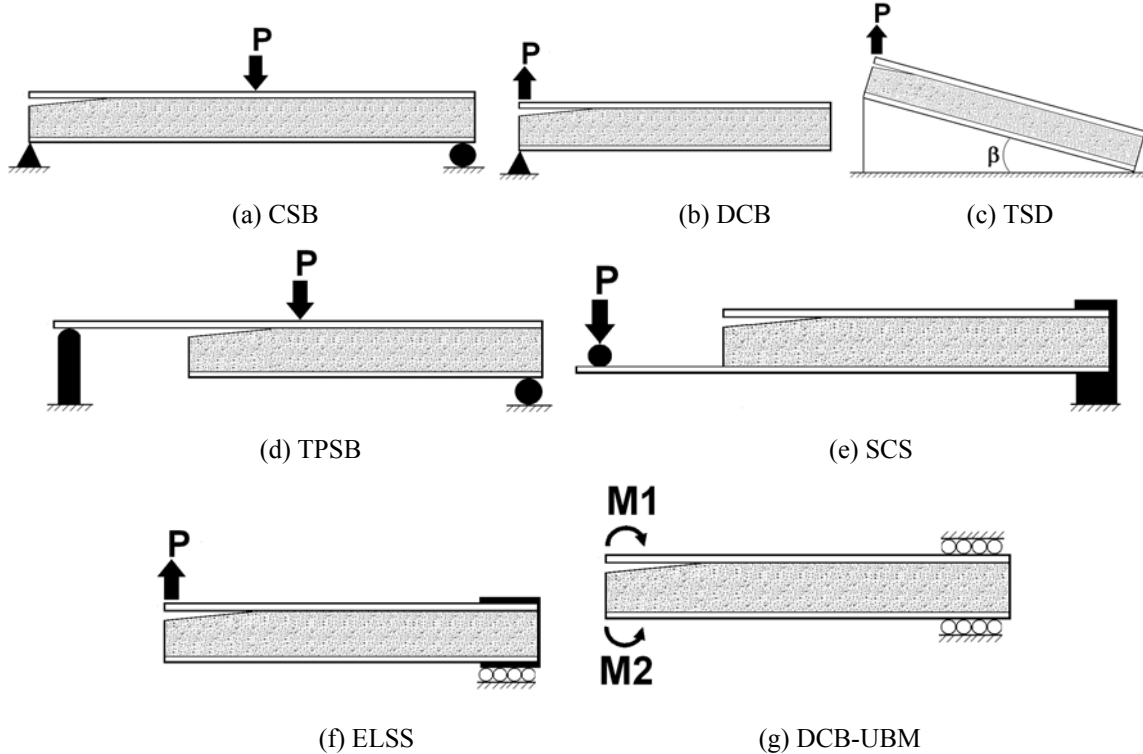

(a) CSB   (b) DCB   (c) TSD

(d) TPSB   (e) SCS

(f) ELSS   (g) DCB-UBM

Fig. 1 Debonded sandwich geometries, a) CSB, b) DCB, c) TSD, d) TPSB, e) SCS, f) ELSS and g) DCB-UBM

The mixed mode bending (MMB) test rig, Fig. 2a, has become a popular test for measuring mixed mode interlaminar fracture toughness of monolithic composite materials [12-16], and has recently become the ASTM standard test method D6671-01 [17]. The standard MMB composite test specimen consists of a rectangular unidirectional beam specimen with a non-adhesive film insert located at the midplane. The MMB test rig allows for alteration of the mixed mode ratio simply by changing the lever arm distance *c* of the apparatus as shown in Fig. 2a. The MMB test rig has also been used for cyclic mixed mode delamination propagation studies for monolithic composites by Sriram *et al.* [18].

However, before approaching studies on crack propagation during cyclic loading it is necessary to establish the suitability of the MMB test as a static mixed mode debond test of sandwich specimens. The MMB test of a debonded sandwich specimen, Fig. 2b, is explored herein.
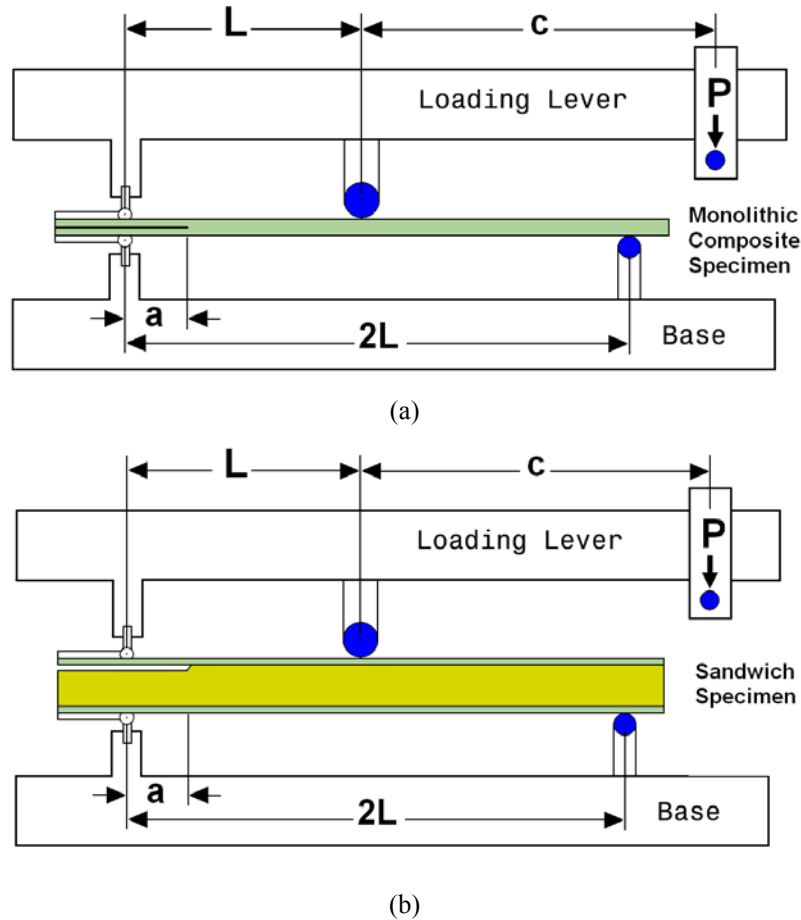

(a)

(b)

Fig. 2 Mixed mode bending fixture a) symmetric monolithic laminated composite, b) sandwich specimen

The objectives of this paper are thus: i) to develop closed-form solutions for the compliance and strain energy release rate for the MMB sandwich specimen, ii) to perform an extensive parametric analysis on the compliance and energy release rate of the MMB sandwich specimen as function of the loading conditions, specimen geometry and material properties, and iii) to perform finite element analysis (FEA) of the MMB sandwich specimen to determine the compliance, energy release rate and local mode mixity at the crack tip for various material combinations and loading conditions.

2   ANALYSIS OF THE DEBONDED SANDWICH SPECIMENS

In this section, the MMB sandwich specimen with an edge crack at the upper face/core interface will be analyzed with the purpose of developing analytic expressions for the compliance and energy release rate. The sandwich specimen is essentially a three-point flexure specimen with a through-width artificial edge crack at the upper face/core interface. The fixture is loaded in compression at a distance *c* from the center, see Fig. 2. Statics analysis of the MMB loading arrangement yields the support reactions at the contact points at the top and bottom surfaces of the MMB specimen. The acting loads and reactions on the sandwich specimen are shown in Fig. 3. *P* is the load applied at a distance *c* (Fig. 2), P_I is the mode I load, P_{II} is the mode II load and P_R is the reaction load at the right end of the MMB specimen.
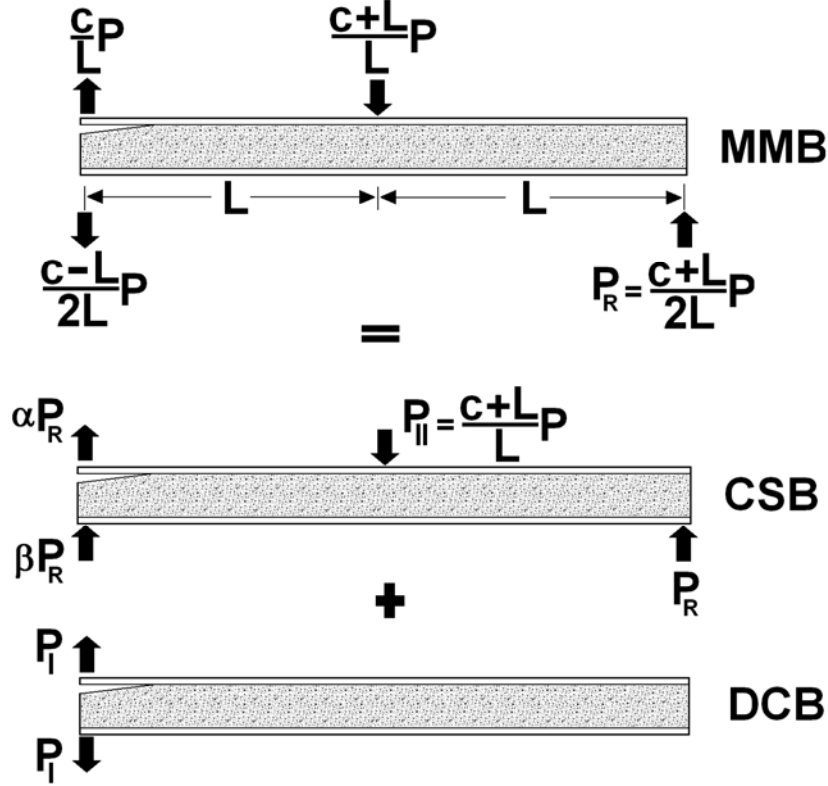

Fig. 3 Mixed mode loading decomposed into CSB and DCB loadings.

It may be recognized that the MMB specimen may be viewed as a superposition of the CSB and DCB specimens, Fig. 1a and 1d. In a macroscopic sense these specimens are pure mode II and pure mode I, respectively, although the bimaterial character of the sandwich interface crack will result in alteration of the mode mixity as discussed later. Partitioning of the overall MMB loading [12] into CSB and DCB loading is illustrated in Fig. 3. The load partitioning may be determined from static equilibrium considerations. Especially the CSB loading requires that part of the vertical reaction load at the left end is supported by the upper face and the remaining part by the lower part of the debonded specimen. Then, the following equilibrium condition must be fulfilled,

$$\alpha P_R + \beta P_R = P_R \tag{1}$$

Early analysis of the monolithic unsymmetric MMB specimen [13] in effect assumes $\alpha=\beta=0.5$ (however without directly using the α, β formulation) and thus neglects the correct load partitioning between the

upper and lower crack flanks. However, for a sandwich specimen this is not valid due to the high stiffness-ratio between the crack flanks.

Consideration of the loads acting on the upper and lower faces at the left edge of the MMB, CSB and DCB specimens in Fig. 3 reveals,

$$\frac{c}{L}P = \alpha P_R + P_I \qquad \text{(upper face)} \qquad (2a)$$

$$\frac{c-L}{2L}P = P_I - \beta P_R \qquad \text{(lower face)} \qquad (2b)$$

Equation (2a) yields,

$$P_I = \frac{c}{L}P - \alpha P_R \qquad (3)$$

and Eq. (2b) just provides a verification of the equilibrium condition at the left end of the sandwich specimen. Furthermore, the mode II load acting on the central part of the specimen is,

$$P_{II} = \left(1 + \frac{c}{L}\right)P \qquad (4)$$

In order to determine the parameters α and β, the debonded region of the beam is assumed to be rigidly built-in into the uncracked part of the specimen, as presented in Fig. 4. It can be visualized that the reaction force, P_R, at the left beam support must be transferred from the lower part of the beam (face + core) to the upper face sheet via contact pressures over the crack interface. This formulation assumes that the load transfer from the lower part of the beam to the upper face sheet in the debonded region through a concentrated forces [7]. This is approximated by application of two concentrated forces αP_R and βP_R applied as illustrated in Fig. 4.
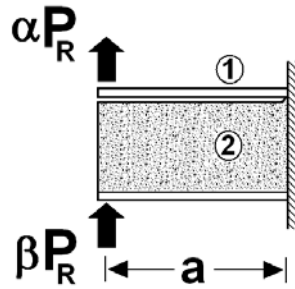

Fig. 4 Load partitioning at the debonded region of the sandwich specimen.

An analysis of the CSB specimen was conducted earlier by Carlsson et al. [7] using first-order shear deformation beam theory and showed that,

$$\alpha = \left[\frac{\dfrac{a^3}{3}\dfrac{1}{D_2} + \dfrac{a}{k}\dfrac{1}{G_f h_f + G_{xz} h_c}}{\dfrac{a^3}{3}\dfrac{1}{D_2} + \dfrac{a}{k}\dfrac{1}{G_f h_f + G_{xz} h_c} + \dfrac{a^3}{3}\dfrac{1}{D_1} + \dfrac{a}{k}\dfrac{1}{G_f h_f}} \right] \tag{5}$$

where the subscripts 1 and 2 refer to the sub-beams (Fig. 4), a is the crack length, k is the shear correction factor, $k=1.2$ [7], $D_2=D-B^2/A$ (lower sub-beam in Fig. 4), $D_1=E_f h_f^3/12$ (upper sub-beam in Fig. 4), h_f is the face sheet thickness, h_c is the core thickness, G_{xz} is the shear modulus of the core, G_f is the shear modulus of the face sheet, E_f and E_c are the face and core moduli [7,19]. The A, B and D terms are the extensional, coupling and bending stiffnesses of any given laminated beam. For the lower beam in Fig. 4, A, B and D (those terms are used to calculate D_2 as well) are given by [7,19]

$$A = E_f h_f + E_c h_c \tag{6a}$$

$$B = h_f h_c \left(\frac{E_c - E_f}{2} \right) \tag{6b}$$

$$D = \frac{1}{12}\left[E_f \left(h_f^3 + 3 h_f h_c^2 \right) + E_c \left(h_c^3 + 3 h_f^2 h_c \right) \right] \tag{6c}$$

Equation (5) yields that only for a symmetric specimen, $\alpha=\beta=1/2$. For a debonded sandwich specimen the lower sub-beam at the cracked region is generally substantially thicker and stiffer than the upper sub-beam, therefore, $\alpha << \beta$.

2.1 Double cantilever beam specimen

The sandwich DCB specimen is shown in Fig. 5. Due to the debond location; the DCB sandwich specimen is unsymmetric. When an upward force P_1 is applied to the debonded upper face, the deflection of the upper and lower legs of the specimen are denoted δ_{DCB_upper} and δ_{DCB_lower}, Fig. 5.
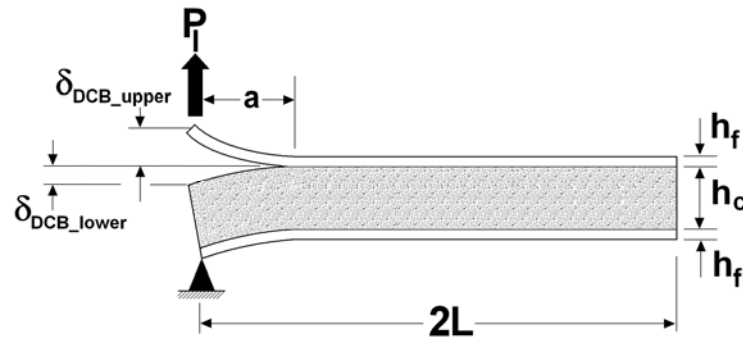

Fig. 5 DCB sandwich specimen

The total displacement of the load application point defines the compliance for the DCB specimen,

$$C_{DCB} = \frac{\delta_{DCB\_lower} + \delta_{DCB\_upper}}{P_I} \tag{7}$$

The DCB sandwich specimen has been analyzed using beam theory combined with an elastic foundation model which is used in order to take into account the elastically built-in configuration of the legs at the crack tip [8,20]. The elastic foundation approach assumes that the uncracked part of the upper face sheet (Fig. 5) is resting on an elastic foundation. Beam theory and elastic foundation provides expressions for the compliance and energy release rate [8].

$$C_{DCB} = C_{DCB\_lower} + C_{DCB\_upper} \tag{8a}$$

$$C_{DCB} = \frac{a}{b}\left[\frac{1}{h_c G_{xz}} + \frac{a^2}{3\left(D - \frac{B^2}{A}\right)}\right] + \frac{4}{E_f h_f^3 b}\left[a^3 + 3a^2\eta^{1/4} + 3a\eta^{1/2} + \frac{3}{2}\eta^{3/4}\right] \tag{8b}$$

$$G_{DCB} = \frac{P_I^2}{2b^2}\left[\frac{1}{h_c G_{xz}} + \frac{a^2}{\left(D - \frac{B^2}{A}\right)} + \frac{12}{E_f h_f^3}\left[a^2 + 2a\eta^{1/4} + \eta^{1/2}\right]\right] \tag{8c}$$

$$\eta = \frac{h_f^3 b E_f}{3K} \tag{8d}$$

where a is the crack length, b is the width of the specimen, P_I is the mode I load and K is the elastic foundation modulus, defined in Ref. [8] as,

$$K = \frac{E_c b}{h_c/2} \tag{9}$$

This equation, in effect assumes that one half of the core is active as a foundation. Increasing the core thickness the elastic foundation modulus decreases. Hence, for very thick cores, the elastic foundation modulus will assume small values, which would prohibit a solution. Since the elastic foundation analysis provides the rotation at the crack tip of the upper face, the elastic foundation modulus should instead include the effect of the face thickness which is actually supported by the elastic foundation. Therefore, a modified elastic foundation modulus for the DCB specimen is proposed,

$$K = \frac{E_c b}{h_f/2} \tag{10}$$

This selection of K is examined in detail in Section 4.1.

8

2.2 Cracked sandwich beam specimen

The loading and geometry of the CSB specimen are shown in Fig. 6. First order shear deformation beam theory was used to analyze the CSB specimen [7].
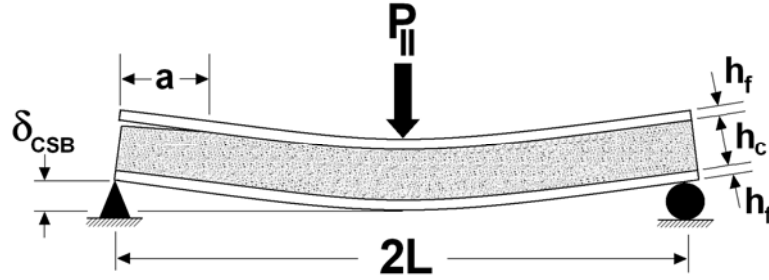

Fig. 6 CSB sandwich specimen

The CSB specimen is loaded in three-point bending and designed to achieve debond propagation along the face/core interface. The compliance and strain energy release rate for a CSB sandwich specimen are given by [7].

$$C_{CSB} = \frac{L^3}{6b\mathrm{D}_{intact}} + \frac{L}{2h_c bG_{xz}} + \frac{a^3}{12b}\left[\frac{1}{\mathrm{D}_{debonded}} - \frac{1}{\mathrm{D}_{intact}}\right] \tag{11}$$

$$G_{CSB} = \frac{P_{II}^2 a^2}{8b^2}\left[\frac{1}{\mathrm{D}_{debonded}} - \frac{1}{\mathrm{D}_{intact}}\right] \tag{12}$$

where L is the half-span length, P_{II} is the mode II load, D_{intact} is the flexural stiffness of the intact region of the beam and $D_{debonded}$ is the effective flexural stiffness of the debonded region of the beam. The flexural stiffnesses of the intact and debonded regions are,

$$\mathrm{D}_{intact} = \frac{E_f h_f}{2}\left(h_c + h_f\right)^2 + \frac{E_f h_f^3}{6} + \frac{E_c h_c^3}{12} \tag{13a}$$

$$\mathrm{D}_{debonded} = \left(1 - \alpha\right)\left(D - \frac{B^2}{A}\right) \tag{13b}$$

where A, B and D are given in Eqs. (6). It may be difficult to propagate the interfacial crack in shear [21,22]. The CSB loading provides an intense shear stress at the crack tip, but the bending of the highly unsymmetric lower part of the debonded region puts the upper surface of the core in compression which may cause core crushing [7,22]. Such difficulties may be expected for the MMB sandwich specimen as well if mode II is dominant. However, careful design of the MMB specimen will promote the desired face/core crack propagation failure mode [23].

2.3 Mixed mode bending specimen

Similar to the original approach by Reeder and Crews [12], the analysis and solutions for the DCB and CSB specimens are here combined in order to develop an analytical expression for the compliance and energy release rate for the MMB sandwich specimen.

Figure 7 shows the kinematics of deformation of the MMB sandwich specimen presented in a form similar to that for unsymmetric composite beams [13]. The dashed line indicates the deformed specimen if only P_I is acting.
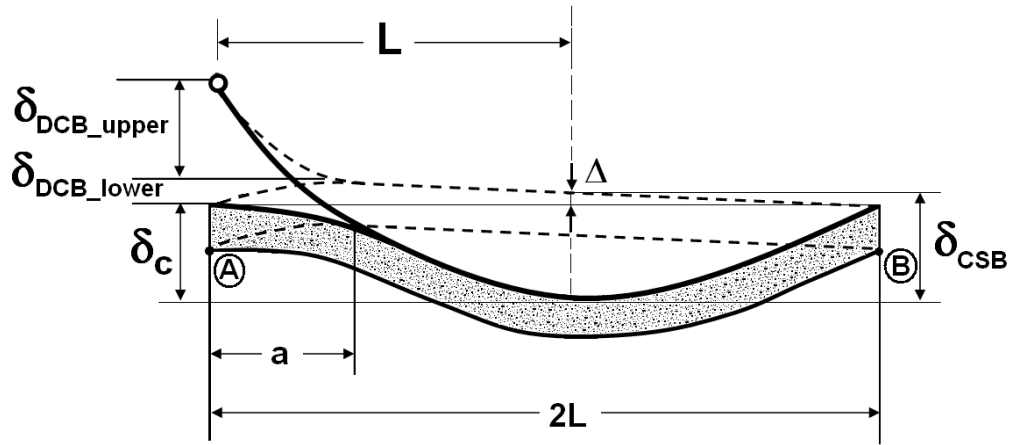

Fig. 7 Kinematic relationship for the MMB sandwich specimen.

The displacement at the center of the beam δ_{CSB} corresponding to the load, P_{II}, with reference to the deformed shape of the mode I loaded specimen is

$$\delta_{CSB} = \Delta + \delta_c \tag{14}$$

This displacement may be visualized as occurring by applying a load of magnitude P_{II} to the deformed specimen loaded by P_I (dashed shape in Fig. 7). The displacement Δ is determined by using the method of similar triangles, as shown in Fig. 7.

$$\frac{\Delta}{L} \approx \frac{\delta_{DCB\_lower}}{2L} \tag{15}$$

Furthermore, δ_{DCB_upper} and δ_{DCB_lower} are the opening displacements of the upper and lower sub-beams of the MMB specimen associated with the mode I opening load P_I as,

$$\delta_{DCB} = \delta_{DCB\_lower} + \delta_{DCB\_upper} \tag{16}$$

The displacement of the point of load application at a distance c from the midpoint of the MMB specimen, see Fig. 8, is given by

$$\delta_{MMB} = \delta_c + \frac{c}{L}\left(\delta_c + \delta_{DCB}\right) \tag{17}$$
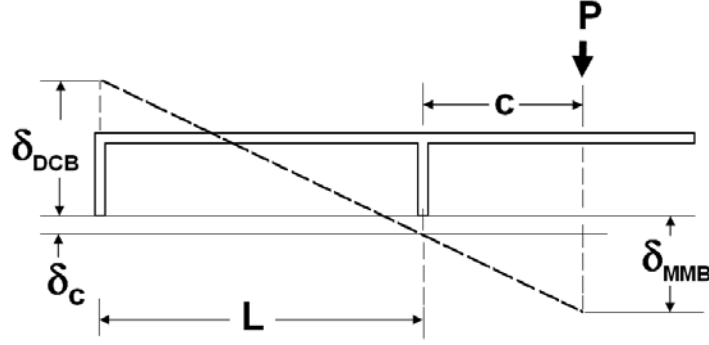
10

Fig. 8 Displacement at the loading point, δ_{MMB}.

Substitution of Eqs. (14)-(16) into (17) yields the following kinematic relationship for the load point displacement

$$\delta_{MMB} = \frac{c}{L}\delta_{DCB\_upper} + \frac{c-L}{2L}\delta_{DCB\_lower} + \left(\frac{c+L}{L}\right)\delta_{CSB} \qquad (18)$$

The displacements δ_{DCB_lower}, δ_{DCB_upper} and δ_{CSB} in Eq. (18) can be expressed in terms of their compliances,

$$\delta_{DCB\_lower} = P_I C_{DCB\_lower} \qquad (19a)$$

$$\delta_{DCB\_upper} = P_I C_{DCB\_upper} \qquad (19b)$$

$$\delta_{CSB} = P_{II} C_{CSB}. \qquad (19c)$$

Combination of Eqs. (19) with (3) and (4) gives the compliance of MMB sandwich specimen,

$$C_{MMB} = \left[\frac{c}{L}C_{DCB\_upper} + \frac{c-L}{2L}C_{DCB\_lower}\right]\left(\frac{c}{L} - \alpha\frac{c+L}{2L}\right) + \left(\frac{c+L}{L}\right)^2 C_{CSB} \qquad (20)$$

Expressions for the compliances C_{DCB_upper}, C_{DCB_lower} and C_{CSB} are given in Eqs. (8b) and (11).

With the compliance determined from Eq. (20), the energy release rate, G_{MMB}, can be expressed as,

$$G_{MMB} = \frac{P^2}{2b}\frac{dC_{MMB}}{da} \qquad (21a)$$

$$G_{MMB} = \frac{P^2}{2b}\frac{d}{da}\left(\left[\frac{c}{L}C_{DCB\_upper} + \frac{c-L}{2L}C_{DCB\_lower}\right]\left(\frac{c}{L} - \alpha\frac{c+L}{2L}\right) + \left(\frac{c+L}{L}\right)^2 C_{CSB}\right) \qquad (21b)$$

$$G_{MMB} = \frac{P^2}{2b^2} \left(\begin{array}{l} \dfrac{c}{L}\left(\dfrac{c}{L} - \alpha\dfrac{c+L}{2L}\right)\dfrac{12}{E_f h_f^3}\left[a^2 + 2a\eta^{1/4} + \eta^{1/2}\right] + \\[3mm] \dfrac{c-L}{2L}\left(\dfrac{c}{L} - \alpha\dfrac{c+L}{2L}\right)\left[\dfrac{1}{h_c G_{xz}} + \dfrac{a^2}{\left(D - \dfrac{B^2}{A}\right)}\right] + \left(\dfrac{c+L}{L}\right)^2\left(\dfrac{a^2}{8}\left[\dfrac{1}{D_{debonded}} - \dfrac{1}{D_{intact}}\right]\right) \end{array} \right) \tag{21c}$$

The global mode ratio is given by $G_{CSB}/G_{DCB} = G_{II}/G_I$

$$\frac{G_{II}}{G_I} = \left(\frac{P_{II}}{P_I}\right)^2\left(\frac{a}{2}\right)^2 \frac{\left[\dfrac{1}{D_{debonded}} - \dfrac{1}{D_{intact}}\right]}{\dfrac{1}{h_c G_{xz}} + \dfrac{a^2}{\left(D - \dfrac{B^2}{A}\right)} + \dfrac{12}{E_f h_f^3}\left[a^2 + 2a\eta^{1/4} + \eta^{1/2}\right]} \tag{22}$$

The methodology presented above is not valid when contact between crack faces is present. Contact arises at a lever arm distance, c, when the mode I load (Eq. (2a)) vanishes. Equation (2a) provides an expression for the minimum lever arm distance c, which is required to avoid contact at the crack faces,

$$c > \frac{\alpha L}{2 - \alpha} \tag{23}$$

For instance, for a symmetric specimen, $\alpha = 1/2$, Eq. (23) gives $c > L/3$ which is generally used as a limit for testing of monolithic composites [12-18] with limited stiffness-ratio between the crack flanks. However, for sandwich specimens, α is very small and therefore the minimum c distance is also very small ($c/L > \alpha/2$) which is convenient in order to expand the range of global mixed mode ratios.

3   FINITE ELEMENT ANALYSIS

Finite element analyses (FEA) of the DCB, CSB and MMB sandwich specimens were performed in order to determine the compliance and energy release rate for different loading conditions, geometries, and material properties. The FEA results will be compared to the compliance and energy release rate predictions using the previously derived analytic expressions. The compliance was calculated by applying a unit load to the sandwich specimens and the energy release rate G was calculated from the relative crack flank displacements (δ_y and δ_x) [24],

$$G = \frac{\pi\left(1 + 4\varepsilon^2\right)}{2x\left(c_1 + c_2\right)}\left(\delta_y^{\;2} + \delta_x^{\;2}\right) \tag{24}$$

where δ_y and δ_x are the opening and sliding relative displacements of the crack flanks at a short distance x behind the crack tip, c_1 and c_2 are stiffness parameters of the materials above and below the bimaterial crack given by,

$$c_m = \frac{k_m + 1}{G_m} \tag{25}$$

where m=material number (i.e. 1=face and 2=core), $\kappa_m=3-4\upsilon_m$ for plane strain and $\kappa_m=(3-\upsilon_m)/(1+\upsilon_m)$ for plane stress, υ_m is Poisson's ratio and G_m is the shear modulus for material m [4,6,25]. The oscillatory index ε can be calculated using the following expression [4,6],

$$\varepsilon = \frac{1}{2\pi}\ln\left(\frac{1-\beta}{1+\beta}\right) \tag{26}$$

where β is a non-dimensional combination of the moduli of the materials above and below the interface as given by Dundurs [25].

$$\beta = \frac{G_1(\kappa_2-1)-G_2(\kappa_1-1)}{G_1(\kappa_2+1)+G_2(\kappa_1+1)} \tag{27}$$

2D finite element models of the DCB, CSB and MMB sandwich specimens were constructed using primarily iso-parametric 4 and 8 node elements (PLANE 42 and 82) in the commercial finite element program ANSYS [26]. The core and face sheet materials are assumed to be isotropic and linear elastic with mechanical properties provided in Table 1. The crack faces in the debonded region were modeled using frictionless contact surfaces (TARGET169 and CONTACT172) in order to prevent the overlapping or interpenetration. Contact surfaces were used also at the points where contact between the specimen and loading or support rollers are present to avoid interpenetration between the loading rollers and the MMB specimen. A highly refined mesh at the crack tip was used to accurately resolve the rapidly changing displacements. The total number of elements used in the FEA model was 6512 and the minimum element size at the crack tip was 5µm (see Fig. 9b). PLANE42 elements defined by 4 corner nodes each with two degrees of freedom were used at the crack tip. This type of element was selected since they can support large strains at the crack tip [26]. The rest of the specimen was constructed with PLANE82 elements defined by 8-nodes having two translational degrees of freedom at each node. Both types of elements were configured in plane strain.

For the determination of the compliance of the DCB an upward unit load per width ($P=(1/b)$ N/mm) was applied and the vertical displacement of the loaded node was recorded. For the CSB specimen a downward unit load was applied at the midpoint node on the top of the specimen and its corresponding displacement recorded. Furthermore, the compliance as well as energy release rate for both specimens was computed for various crack lengths. In the FEA of the MMB specimen, the reaction loads are applied as depicted in Fig. 9a.
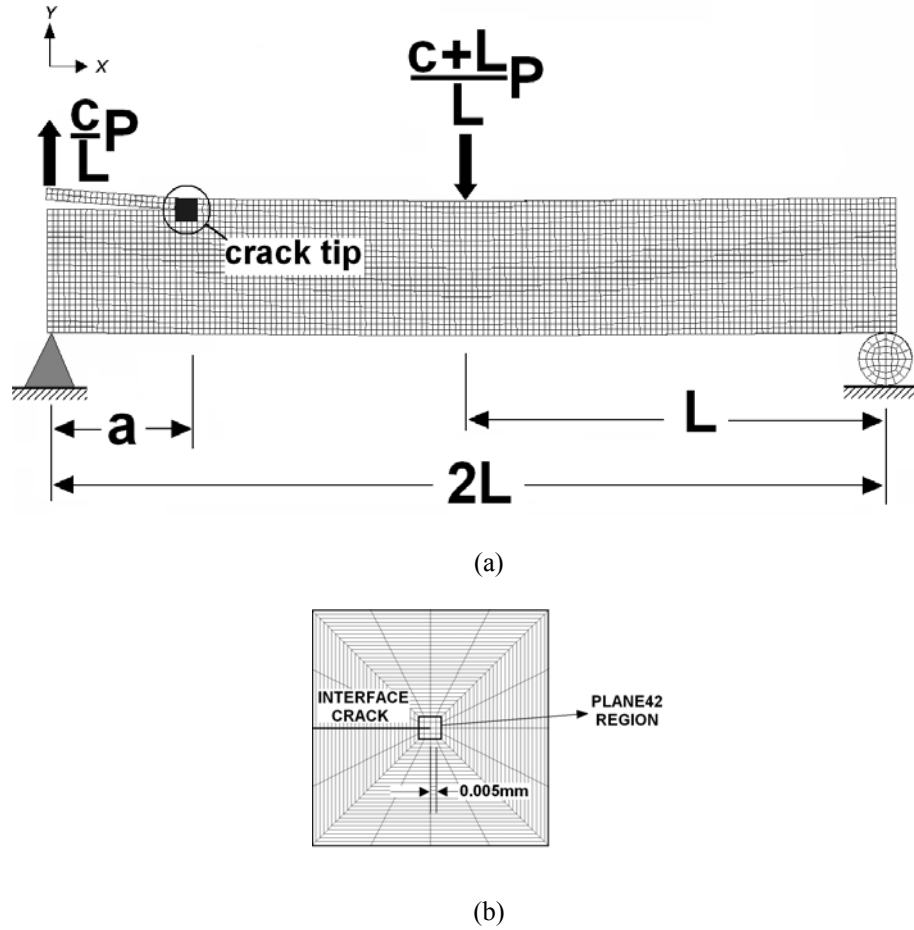
(a)

(b)

Fig. 9 a) Finite element model of the MMB sandwich specimen and b) crack tip details.

4   NUMERICAL ANALYSIS AND CALIBRATION

Generally the critical energy release rate required to propagate a crack (i.e. fracture toughness) is dependent on the mode ratio. A small change in the compliance can cause an over or under prediction in the energy release rate since this is obtained from the derivative of the compliance. Due to this reason, for a mixed mode bending case it is important to accurately predict the compliance and energy release rate.   The accuracy of the analytical expressions for the DCB, CSB and MMB specimens will thus be examined.

4.1 Double cantilever beam specimen

The accuracy of the analytical DCB model to predict the compliance and energy release rate were evaluated using FEA. A set of specimens of total length $2L$ of 150mm, b=35mm, h_f=2mm and core thicknesses h_c of 10, 20, and 30mm were analyzed over a range of crack lengths from 5 to 65mm. The face and core material were typical non-crimp quadro-axial E-glass/polyester mats and H100 PVC foam with properties provided in Table 1. The compliance and energy release rate results determined from the elastic foundation model, Eqs. (8), with the foundation modulus given in Eq. (9) and (10), and FEA are shown vs. crack length in Figs. 10 and 11. The energy release rate was calculated using a unit load per width of the specimen, P=($1/b$) N/mm. The compliance and energy release rate predictions using an elastic foundation modulus of

$K=(E_cb)/h_c/2$ (Eq. (9)) exceed the FEA results, especially for larger core thicknesses and longer crack lengths. However, $K=(E_cb)/h_f/2$ (Eq. (10)) brings the foundation model in excellent agreement with FEA for each of the sandwich materials and geometries considered.

Results in Fig. 10 presents the DCB compliance for three different core thicknesses with constant face sheet thickness and it is observed that the compliance does not exhibits strong dependency on the core thickness. This is attributed to the fact that the directly loaded face sheet thickness is more compliant than the lower sub-beam (core + face sheet) and thus dominated by the directly loaded compliant face sheet. The same trend is observed for the energy release rate results presented in Fig. 11 and the rationale behind that behavior is the same as for the compliance. Furthermore, Figs. 10 and 11 show that the DCB specimen compliance and energy release rate are larger for increasing crack length.
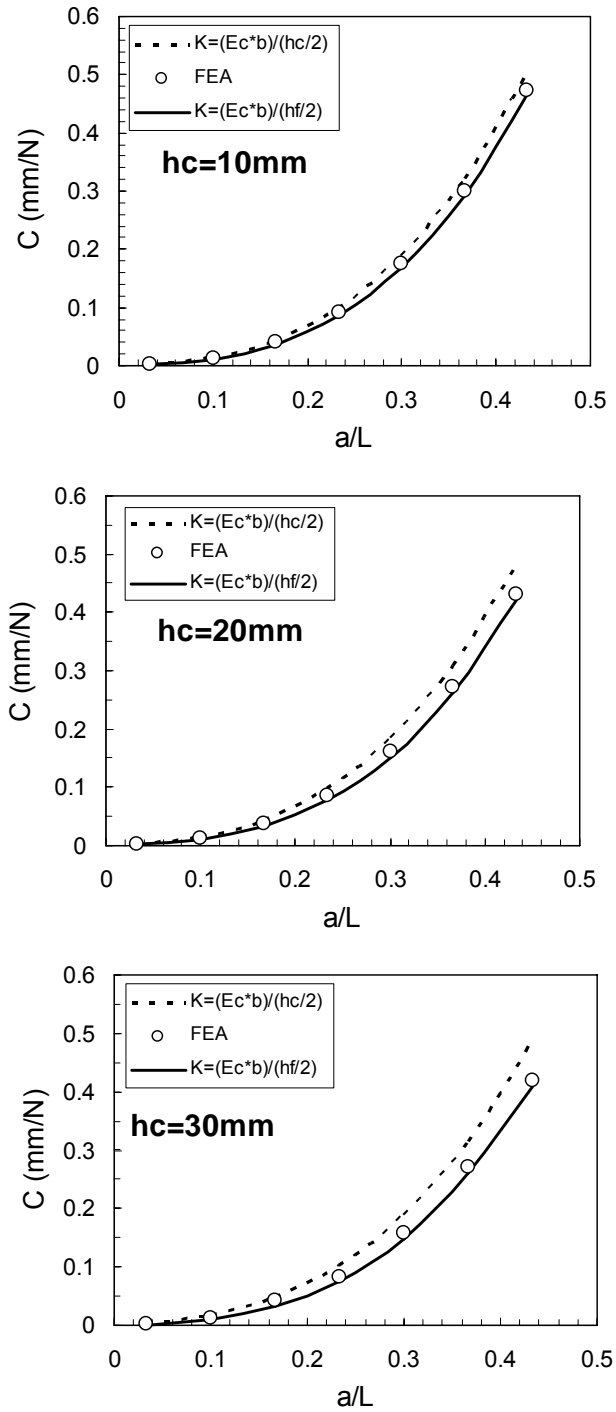
Fig. 10 Core thickness effect on the compliance of DCB sandwich specimens. Open circles represent FEA, and dotted and continuous lines the elastic foundation model.
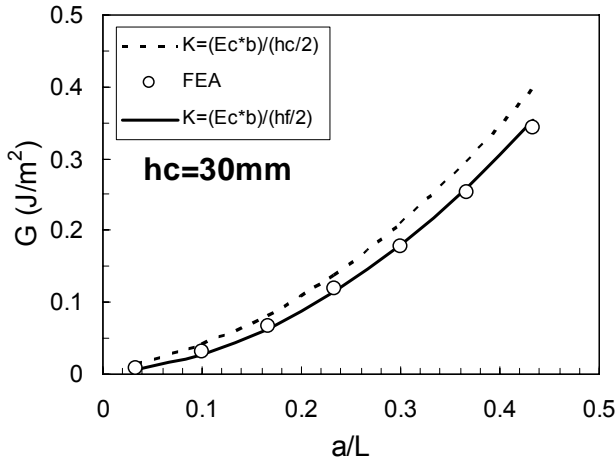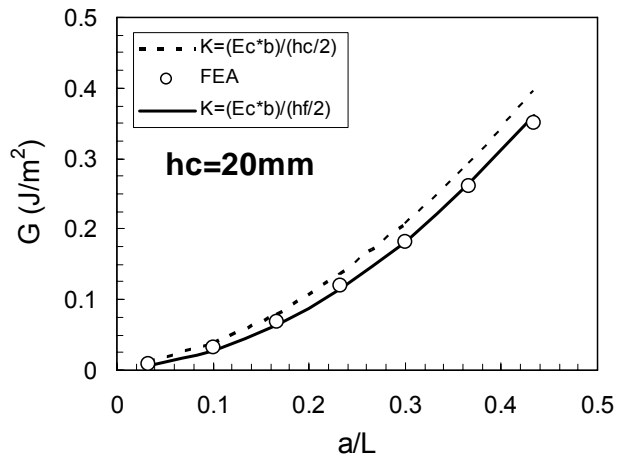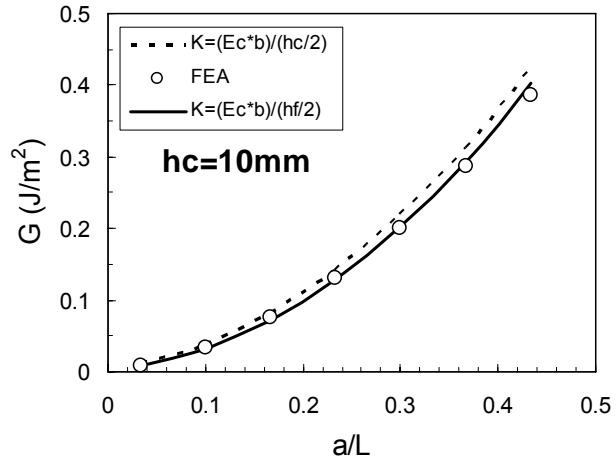
Fig. 11 Core thickness effect on the energy release rate of DCB sandwich specimens. Open circles represent FEA, and dotted and continuous lines the elastic foundation model.

4.2 Cracked sandwich beam specimen

The same materials and geometries as in the analysis of the DCB specimen (Section 4.1) were used in the finite element analysis of the CSB specimen. Analytical (Eqs. (11) and (12)) and finite element results for the compliance and energy release rate (calculated using $P=(1/b)$ N/mm) versus crack length for the CSB specimen are presented in Figs. 12 and 13.
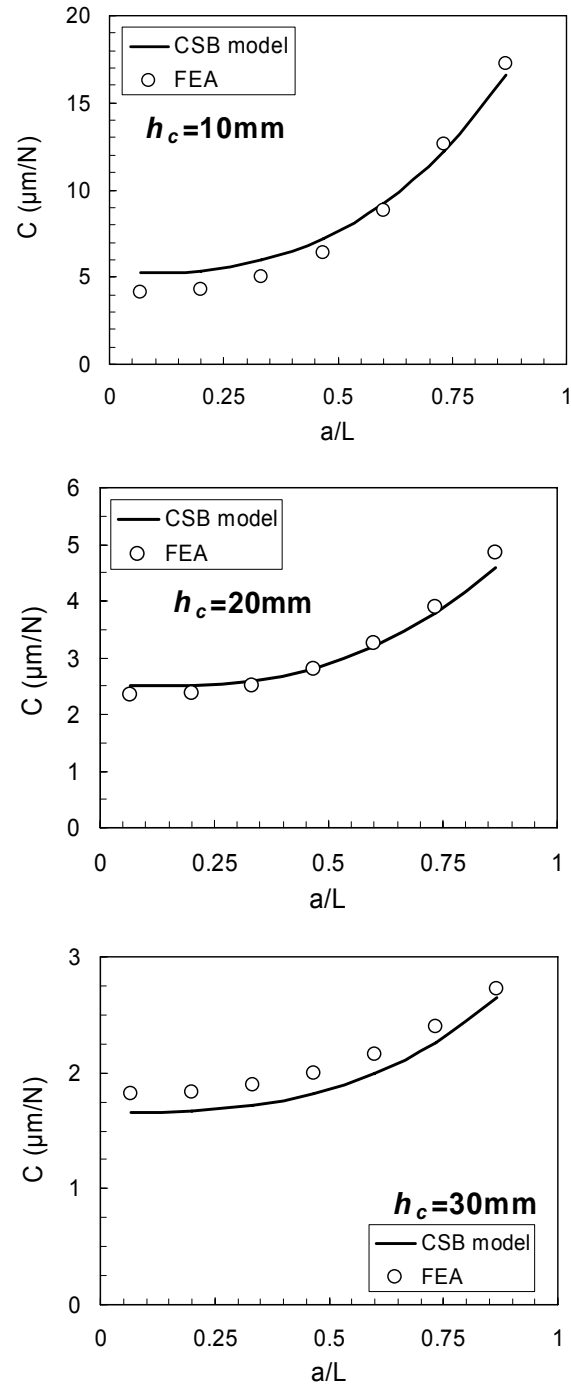

Fig. 12 Core thickness effect on the compliance of CSB sandwich specimens. Open circles represent FEA and continuous lines the beam model.

Fig. 13 Core thickness effect on the energy release rate of the CSB sandwich specimens. Open circles represent FEA and continuous lines the beam model.

Figure 12 shows compliance results. The CSB compliance determined analytically, Eq. (11), and numerically agrees well except for shorter crack lengths. At short crack length the deviation might be caused by the increasing shear deformation of the core [7]. In addition, the influence of the core thickness

on the CSB compliance is significant; larger core thicknesses enhance the CSB flexural stiffness and thus reduce the compliance. For the energy release rate, Fig. 13, it is observed a strong dependency on the crack length at any length, and large energy release rate values are associated to CSB specimens with thin cores since a sandwich specimen with thin cores are more compliant. Furthermore, a very good agreement between the predictions from beam theory and FEA is noted. Small differences could be attributed to the contact pressure developed at the debonded region between the upper and lower sub-beams. The analytical formulation models load transfer from the lower part of the beam to the upper face sheet in the debonded region trough a concentrated force [7,22]. On the other hand, the finite element model includes frictionless contact surfaces between the upper and lower sub-beams in order to achieve load transfer for the debonded region. The two contact definitions are not identical, and small variations between these two models might be expected, as observed in Figs. 12 and 13.

4.3 Mixed mode bending specimen

This section presents a comparison between FEA and the analytic model to predict the MMB compliance and energy release rate and then performs a parametric study, as presented Section 5. FEA of the MMB sandwich specimen was likewise performed. The material and dimensions used for the analysis are the same as for the CSB and DCB specimens. Three core thicknesses (i.e. 10, 20 and 30mm) and a range of crack lengths were examined. A lever arm distance of c=25mm was used for this part of the analysis.

Fig. 14 Core thickness effect on the MMB compliance, h_f=2mm. Open circles represent FEA and continuous lines the beam model.

20

Figure 14 shows that the analytical and FEA compliance results are in good agreement. The energy release rate as function of crack length for three core thicknesses is shown in Fig. 15. The predictions from the beam analysis and FEA are again in close agreement.
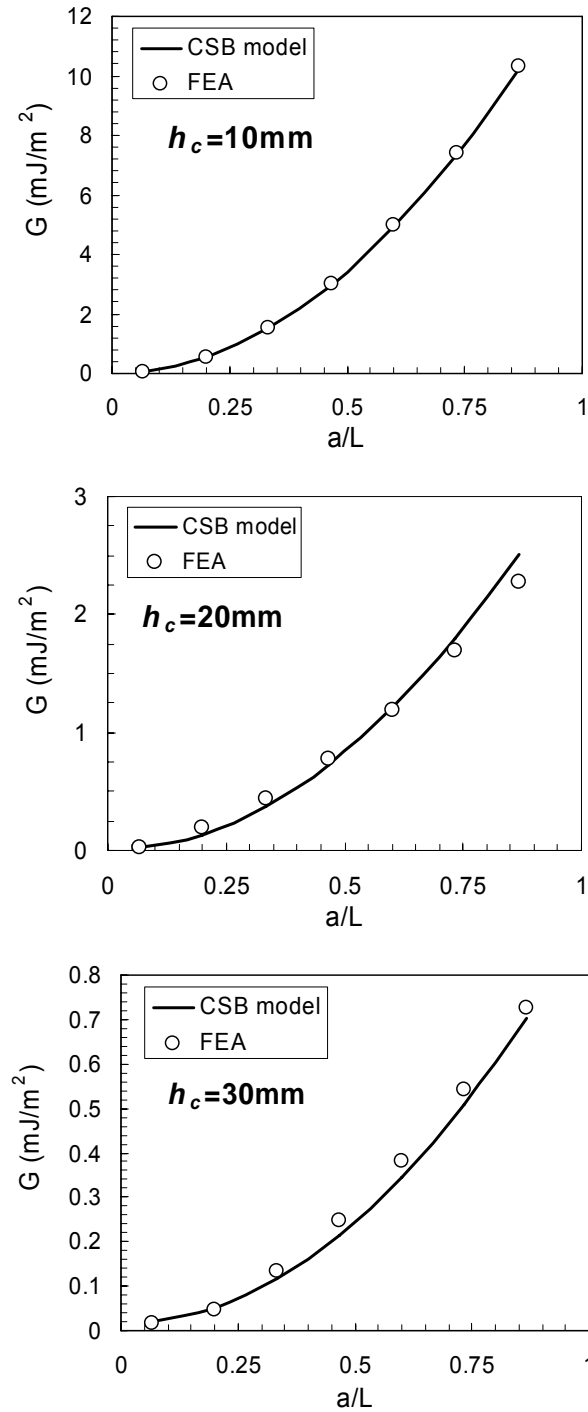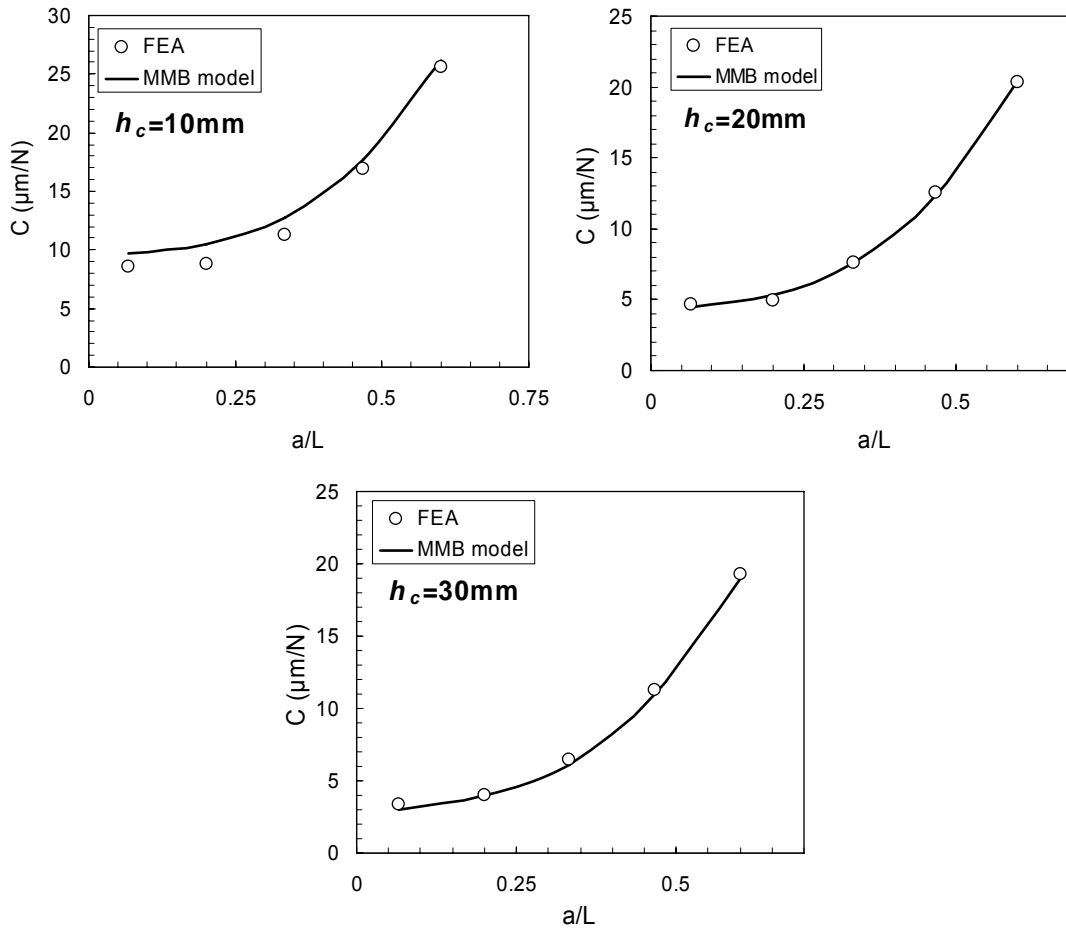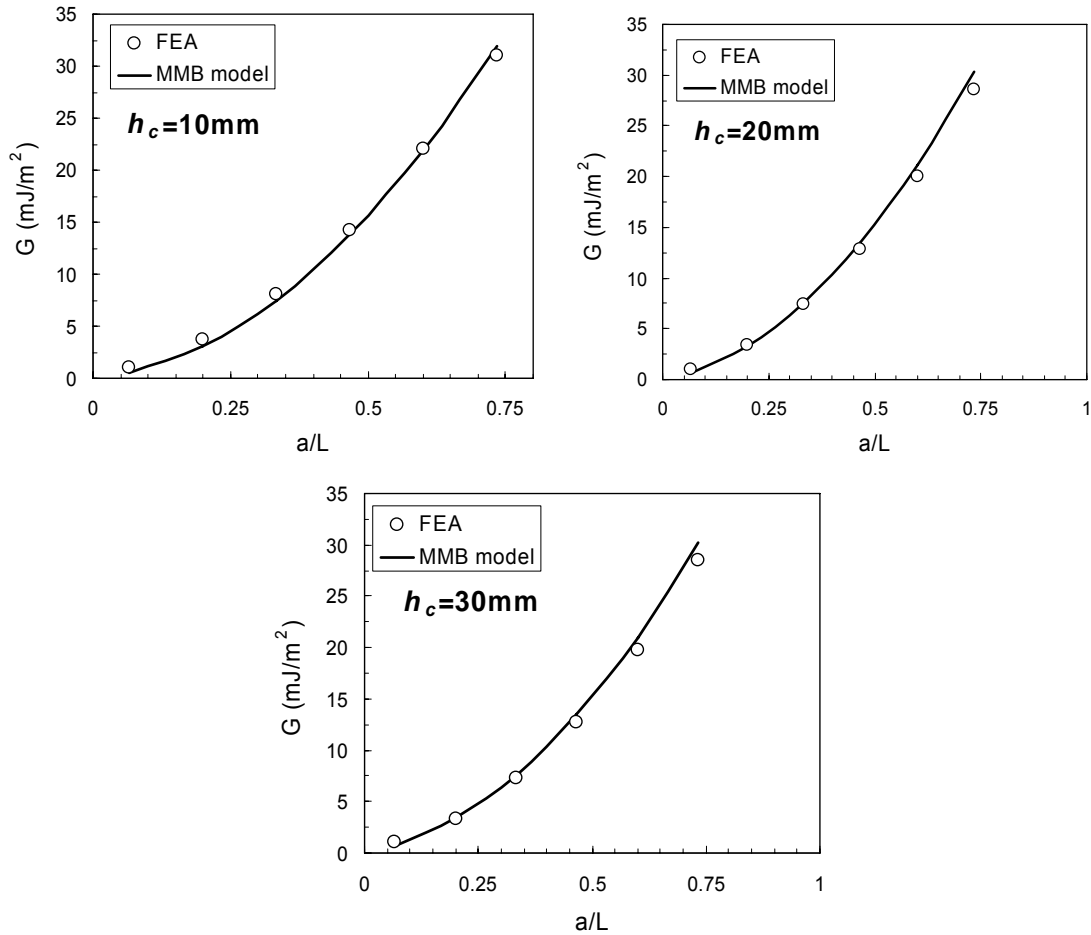

Fig. 15 Core thickness effect on the MMB energy release rate. Open circles represent FEA and continuous lines the beam model.

As observed in Fig. 14, the MMB compliance increases for increasing crack length, especially at long cracks. In addition, Fig. 14 reveals that for increasing core thickness the MMB compliance decreases significantly. This is caused by the increased flexural stiffness for sandwich specimens with ticker cores, as observed early for the CSB specimens. For the energy release rate, results in Fig. 15 exposes that energy release rate in strongly influenced by the crack length. Furthermore, increasing core thickness (from 10 to 30 mm) does not affect significantly the energy release rate in the MMB specimen.

5   PARAMETRIC ANALYSIS OF THE MIXED MODE BENDING SANDWICH SPECIMEN

A parametric study was conducted to examine the influence of mixed mode loading, specimen geometry and material properties on the MMB compliance and energy release rate. The parametric analysis of the loading condition was performed by varying the distance c to vary the relative amount of mode I and mode II loading. To evaluate the influence of the core and face sheet thicknesses, they were varied from 10-30mm and 1-3mm, respectively. The effect of core mechanical properties on displacement, compliance and

energy release rate was studied for three PVC closed-cell foam core materials with properties listed in Table 1.

Table 1 Mechanical properties of face and core materials [5,27,28]

	E_x, MPa	G_{xz}, MPa	v_{xz}	Density kg/m^3	G_{IC} * J/m^2
Face sheets DBLT-850	16400	2700	0.17	-	-
PVC foam H45	50	15	0.325	45	150
PVC foam H100	135	35	0.325	100	310
PVC foam H200	240	85	0.325	200	625

* Fracture toughness

Mixed mode loading is controlled by varying the length of the lever arm, c. The compliance and energy release rate for a specific sandwich geometry (L=75mm, b=35mm, h_c=30mm, h_f=2mm and a=25mm) were determined using Eqs. (20) and (21c) and FEA for lever arm distances c=20, 30, 40 and 50mm. The sandwich employed a H100 foam core and DBLT-850 face sheet with the properties listed in Table 1. The results from FEA and analytic predictions (Eqs. (20) and (21c)) for the compliance and energy release rate ($P=(1/b)$ N/mm) are provided in Table 2.

Table 2 MMB compliance and energy release rate, h_f=2mm, h_c=30mm.

c (mm)	20	30	40	50
C_{FEA}- $\mu m/N$	3.41	6.2	9.7	14.2
$C_{Analytic}$- $\mu m/N$	3.60	6.3	9.9	14.6
G_{FEA}-(mJ/m^2)	2.37	5.6	10.1	16
$G_{Analytic}$-(mJ/m^2)	2.5	5.3	9.71	14.7
G_{II}/G_I	0.038	0.02	0.014	0.01

The compliance and energy release rate obtained from beam analysis and FEA are in good agreement for the range of c values analyzed. Both compliance and energy release rate increase with increasing lever arm distance c since mode I become dominant. Furthermore, the mode ratio (G_{II}/G_I) (Eq. (22)) decreases as the distance c increases, indicating more mode I dominance. While the correlation for the DCB is slightly better than CSB when compared against FEA, it is expected slightly improved correlation for mixed mode loadings with mode I dominant, as observed in Table 2.

To examine the influence of changes in face and core thicknesses, face sheet thicknesses of 1, 2 and 3mm and core thicknesses of 10, 20 and 30mm were examined. The specimen geometry was $2L$=150mm, b=35mm, a=25mm and c was held constant at 30mm. MMB compliance and energy release rate results obtained analytically and from FEA are presented in Tables 3 and 4.

The results in Table 3 show that the MMB specimen with thin face sheets are very compliant and large displacements during testing can be expected. The face sheet thickness has a strong influence on the energy release rate. Thin faces results in high energy release rate values which have similar effect that increasing distance c. In addition, for the specimen with 1mm thick face sheets, the mixed mode ratio is very small (0.0098) (mode I dominant). For larger face sheet thickness the mode ratio increases substantially which is associated to an increased mode II loading, and thus larger G_{II}/G_I.

Table 3 MMB compliance and energy release rate for various face thicknesses, h_c=20mm, c=30mm

h_f (mm)	1	2	3
C_{FEA}- $\mu m/N$	26.5	6.8	4.3
$C_{Analytic}$- $\mu m/N$	28.4	6.8	4.7
G_{FEA}-(mJ/m^2)	43	5.34	1.95
$G_{Analytic}$-(mJ/m^2)	38	5.6	1.9
G_{II}/G_I	0.0098	0.063	0.177

The influence of the core thickness, h_c, is examined. Compliance and energy release rate results for the MMB specimens with h_c=10, 20 and 30mm are listed in Table 4.

Table 4 MMB compliance and energy release rate for various core thicknesses, h_f=2mm, c=30mm

h_c (mm)	10	20	30
C_{FEA}-$\mu m/N$	9.5	6.8	6.2
$C_{Analytic}$- $\mu m/N$	10.8	6.8	6.3
G_{FEA}-(mJ/m^2)	5.67	5.34	5.3
$G_{Analytic}$-(mJ/m^2)	5.4	5.6	5.6
G_{II}/G_I	0.44	0.063	0.02

It is noted that the core thickness influences the compliance, decreases as core thickness increases, but has a very small effect on the energy release rate. The results in Table 4 also reveal that the mode ratio, G_{II}/G_I, decreases with increasing core thickness since thicker cores promote dominant mode I loading (thick cores elevates the flexural stiffness in sandwich composites). In summary, thick cores will promote dominant mode I loadings while thin cores the opposite.

The effect of the mechanical properties of the foam core on the compliance and energy release rate of the MMB specimen was analyzed. It has been reported previously that reducing the face modulus has a similar effect on the compliance and energy release rate as changing the face thickness [7]. The face thickness effect on the compliance and energy release rate was presented above in Tables 3 and 4.

Three foams, viz. H45, H100 and H200 were examined (Table 1). The face sheet modulus E_x, was kept constant (Table 1). The specimen geometry used for this analysis was b=35mm, $2L$=150mm, a=25mm, h_f=2mm, h_c=30mm and the lever arm distance was c=30mm. The results in Table 5 reveal that the core modulus has a strong influence on the compliance which decreases markedly with increasing core modulus, while the energy release rate decreases only slightly. Moreover, the mode ratio decreases with increasing core stiffness.

Table 5 MMB compliance and energy release rate for various PVC foam cores, E_c.

E_c, MPa	50	135	240
C_{FEA}- $\mu m/N$	9.3	6.2	4.4
$C_{Analytic}$- $\mu m/N$	9.5	6.3	4.8
G_{FEA}-(mJ/m^2)	6.18	5.3	4.83
$G_{Analytic}$-(mJ/m^2)	6.2	5.6	5
G_{II}/G_I	0.048	0.02	0.012

As a final point in this section, the global mixed mode ratio (Eq. (23)) was examined for the MMB specimens with $2L$=150mm, b=35mm, h_f=2mm, h_c=30mm, c=40mm over a range of crack lengths. This analysis was conducted in order to evaluate the influence of crack length and core modulus on the global mode ratio, G_{II}/G_I. The results are presented in Fig. 16. For specimens with H100 and H200 cores, the global mixed mode ratio is approximately constant for $a/L \geq 0.2$. However, for the specimen with H45 core, the global mixed mode ratio is not constant and an increasing trend in observed as the crack length increases. It is believed that the first order shear deformation beam theory employed to develop the MMB expressions do not predict accurately the deformations of the very soft H45 foam core and high order shear deformation theories can be explored (out of the scope of the paper). However, since the error in predicting the total energy release rate using Eq. (21c) when compared to FEA is less than 10% (assuming FEA as the exact solution), as presented earlier, the model is considered accurate enough for engineering purposes.
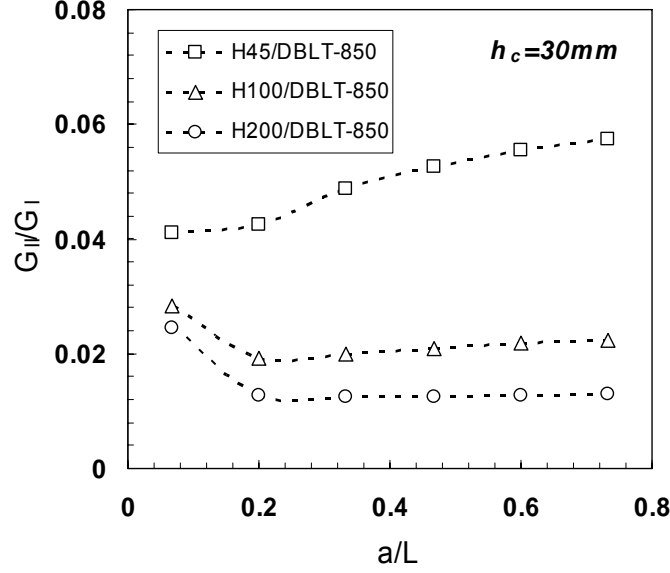
Fig. 16 Global mixed mode ratio versus debond length for various core materials (E-glass fiber DBLT-850 face material) with h_f=2mm and h_c=30mm.

6   LOCAL MODE MIXITY AT THE CRACK TIP

It is important to point out that the global mode mixity differs from the local crack tip mode mixity [4,24,29]. The local mode mixity arises due to the fact that the crack propagates at or near a bimaterial interface between two widely different materials with a high stiffness mismatch. The bimaterial character of the interface influences the mode mixity at the crack tip because tensile and shear stresses must appear along the interface to maintain continuity in displacement between the core and face sheet. The local mode mixity depends on the external loads applied to the specimen and the material properties above and below the interface. The local mode mixity is expressed as a phase angle which measures the relative amount of mode II to mode I [4,24]. The local mode mixity at the interface crack can be defined from the opening δ_y and sliding δ_x relative displacements of the crack flanks at a short distance x behind the crack tip,

$$\psi = \tan^{-1}\left(\frac{\delta_x}{\delta_y}\right) - \varepsilon \ln\left(\frac{x}{h}\right) + \tan^{-1}(2\varepsilon) \tag{28}$$

where h is a characteristic distance, here set equal to the face sheet thickness, and ε is defined in Eq. (26). The relative displacements can be determined from FEA. The local mode mixity at the crack tip is here determined by using the crack surface displacement extrapolation (CSDE) method which has been proven to be efficient and reliable for sandwich face/core interfaces [3,30]. The CSDE method calculates the phase angle, ψ, from nodal displacements along the crack flanks and extrapolates the found values to the crack tip ($x \rightarrow 0$). For more details, see [3,30].

To obtain the local mode mixities at the crack tip, FEA was conducted to determine the phase angle ψ (Eq. (28)). Three foam core materials (H45, H100 and H200) and DBLT-850 face sheets (Table 1) were used in the analysis of the local mode mixity. A MMB specimen with b=35mm, h_f=2mm, h_c=30mm, $2L$=150mm was considered. A range of normalized crack lengths, a/L, from 0.07 to 0.73 was examined. The effects of core thickness, h_c, and core modulus E_c on the mode mixity were examined. Core thickness h_c was varied between 10-30mm and h_f=2mm (i.e. h_c/h_f =5, 10 and 15). The core modulus E_c was varied from 50 to 240MPa and the face modulus was kept constant (Table 1).

24

The influence of crack length on the local mode mixity is shown in Fig. 17a. It can be observed that the phase angle is roughly constant for $a/L > 0.2$. This observation is important for fatigue tests at constant mode mixities. However, at very small crack length ($a/L < 0.2$) the mode mixity is not constant. Earlier studies on the CSB sandwich specimen with very short crack lengths revealed core shear failure prior crack extension and thus significant shear deformation [7]. While specimens with very short crack deforms similarly to an uncracked specimens, the shear deformation at the core (knowing that the shear stresses are almost entirely carried by the core) might be nonlinear to could alter the mode mixity at the crack tip that causes a rapid change in the mode mixity as the crack increases up to $a/L=0.2$. Since the global mixed mode ratio (G_{II}/G_I) is constant for cracks larger than $a/L \geq 0.2$, thus the mode mixity remains roughly constant as well, in accordance with the behavior observed in Fig. 16, especially for the H100 and H200 cores. For the case of H45 core, the G_{II}/G_I is not constant as observed in Fig. 16, however, the mode mixity determined from finite element reveals a constant mode mixity for $a/L \geq 0.2$, as observed in Fig. 17a. This is because the FE model can accurately capture the deformation in the core and at the crack tip. Therefore, it is suggested to use an initial crack length $a/L \geq 0.2$ that promotes approximately constant local mode mixity. As a reference, the ASTM standard [17] for delamination characterization of monolithic laminated composites recommends an initial delamination length $a/L \approx 0.4$.

Figure 17b shows the effect of the core thickness on the phase angle. As the core thickness (ratio h_c/h_f) increases, the mode mixity becomes less negative. This indicates that for thicker cores the crack tip loading becomes more mode I dominated. Figure 17c shows that as the core modulus, expressed as the E_c/E_f ratio, increases, the phase angle increases, but only for large c/L ratios.

The effect of the lever arm distance c (c/L) on the local mode mixity at the crack tip is specifically presented in Fig. 17d. The results show that the phase angle becomes less negative (more mode I) as the c/L ratio increases. Furthermore, the phase angle is quite sensitive to changes of c at small c values, especially for small core thicknesses. The crack length needs to be specified when you change lever arm distance, c. Thus, the lever arm distance c or c/L has a strong effect on the local mode mixity at the crack tip.

In order to achieve a full set of phase angles, it is recommended to use different specimen dimensions (i.e. ratios h_c/h_f), for instance thick cores (large h_c/h_f) and large c distances promotes dominant mode I loading, whereas, thin core (small h_c/h_f) and small c values mode II loading. Furthermore, further analysis regarding the competing failure modes such as core shear, indentation at load introduction and supports and core crush at the crack tip need to be performed. Thus, those undesired failure modes can be avoided in order to promote debond propagation as controlling failure mechanism in the MMB specimen.
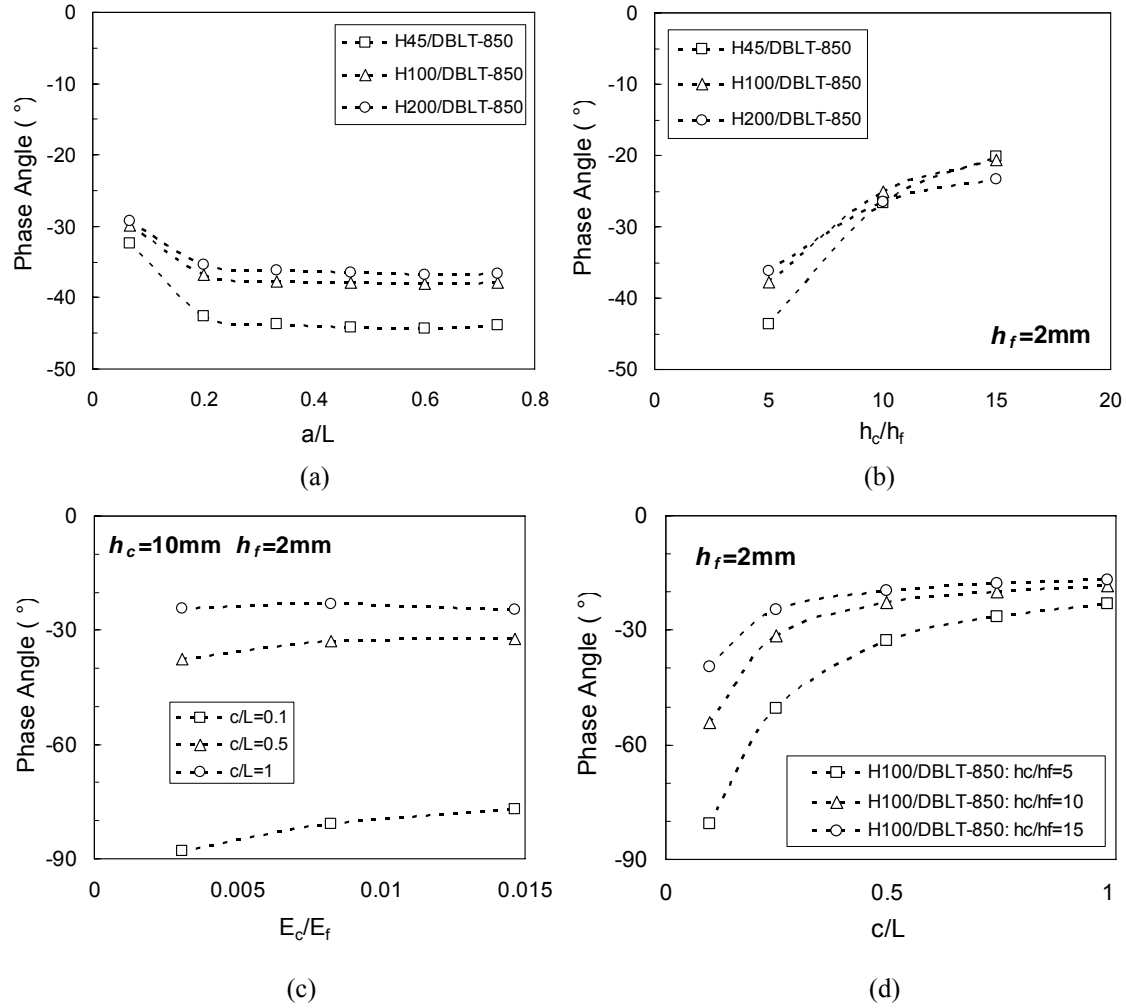
Fig. 17 Phase angle as function of: a) normalized crack length, b) core-to-face thickness ratio, c) core-to-face modulus ratio, and, d) normalized lever arm distance and h_c/h_f ratios.

Finally, the limitation of the MMB model is when contact between crack faces is present and occurs when mode I load vanishes. In order to avoid this contact problem at the crack faces, Eq. (23) provides a limiting minimum c value that can be used in the MMB model. Pure mode I loading at the crack tip, $\psi=0°$, can not be achieved even using large c values because a small mode II loading is still present. Pure mode II loading, $\psi=-90°$, can not be achieved either due to contact between the crack faces. However, in the literature there is no testing methodology available that can perform pure mode I or mode II loadings in sandwich specimens. Therefore, despite these limitations for the MMB model, it is still very attractive and applicable for mixed mode testing under a wide range of mode mixities, i.e. dominant mode I and mode II loadings. Moreover, the current MMB model works very well for isotropic face sheets and cores. Quadro-axial ($E_x = E_y$) face sheets with isotropic cores can be analyzed as well, since the loading of the MMB specimen is mainly in flexure; the material property needed for the analysis will be the elastic modulus in direction E_x and G_{xz}. This was verified by running finite element analysis and comparing the results with MMB model predictions (not presented here), and the results showed good agreement, similar to the analysis presented above.

7 CONCLUSIONS

The analysis of the mixed mode bending sandwich specimen has been presented and validated using finite elements. The analysis utilizes previously derived expressions for the compliance of DCB and CSB specimens, and superimposes those solutions into solutions for the compliance and energy release rate of the MMB specimen. The predictions of the compliance and energy release rate using the analytic and FEA solutions are in good agreement. The present study showed that the compliance and strain energy release rate for the MMB specimen depend quite strongly on geometry, loading conditions and mechanical properties of the sandwich constituents. A lower bound on the lever arm distance c to prevent contact of the crack flanks is derived for debonded sandwich specimens. This expression reveals that the sandwich MMB specimen can be tested at short crack lengths before contact occurs. However, short initial crack lengths, $a/L < 0.2$, should be avoided because the rapidly changing phase angle. The local mode mixity showed low sensitivity to changes in crack length ($a/L \geq 0.2$). As for the monolithic composite MMB specimen, mode I dominated loading can be achieved by using a large distance, c, for load application. A high core thickness similarly promotes mode I dominance, while changes in the core modulus produce quite small changes in the mode mixity. The formulation developed can be applied to any combination of isotropic face and core materials as well as quadro-axial face sheets, and their thickness and the test geometry can be tailored to achieve a large range of (negative) phase angles.

ACKNOWLEDGEMENTS

REFERENCES

[1]   Shipsha A., Burman M. and Zenkert D. Interfacial Fatigue Crack Growth in Foam Core Sandwich Structures. *Fatigue and Fracture of Engineering Materials,* 22:123-131, 1999.

[2]   Nøkkentved A., Lundsgaard-Larsen C. and Berggreen C. Non-Uniform Compressive Strength of Debonded Sandwich Panels - I. Experimental Investigation. *Journal of Sandwich Structures and Materials*, 7(6):461-482, 2005.

[3]   Berggreen C. and Simonsen, B.C. Non-Uniform Compressive Strength of Debonded Sandwich Panels - II. Fracture Mechanics Investigation. *Journal of Sandwich Structures and Materials*, 7(6):483-517, 2005.

[4]   Leichti K.M. Chai Y.S. Asymmetric Shielding in Interfacial Fracture Under In-Plane Shear. *Journal of Applied Mechanics*, 59:295-304, 1992.

[5]   Berggreen C. *Damage Tolerance in Debonded Sandwich Structures*, PhD. Thesis, Department of Mechanical Engineering, Technical University of Denmark, 2004.

[6]   Cao H.C. and Evans A.G. An Experimental Study of the Fracture Resistance of Bimaterial Interfaces. *Mechanics of Materials*, 7:295-304, 1989.

[7]   Carlsson L.A., Sendlein L.S. and Merry S.L. Characterization of Face/Core Shear Fracture of Composite Sandwich Beams. *Journal of Composite Materials*, 25(1):101-116, 1991.

[8]   Avilés F. and Carlsson L.A. Analysis of the Sandwich DCB Specimens for Debond Characterization. *Engineering Fracture Mechanics*, 75:153-168, 2008.

[9]   Li X. and Carlsson L.A. Fracture Mechanics Analysis of the Tilted Sandwich Debond (TSD) specimen. *Journal of Composite Materials*, 35 (23): 2145-2168, 2001.

[10] Ratcliffe J. and Cantwell W.J. Center Notched Flexure Sandwich Geometry for Characterizing Skin-Core Adhesion in Thin-Skinned Sandwich Structures. *Journal of Reinforced Plastic and Composites*, 20(11): 945-970, 2001.

[11] Sørensen B.F., Jørgense K., Jacobsen T.K. and Østergaard R.C. DCB-specimen Loaded with Uneven Bending Moments. *International Journal of Fracture*, 141:163-176, 2006.

[12] Reeder J. and Crews J.H. Mixed-Mode Bending Method for Delamination Testing. *AIAA Journal*, 28(7):1270-1276, 1990.

[13] Ozdil F. and Carlsson L.A. Characterization of Mixed Mode Delamination Growth in Glass/Epoxy Composite Cylinders. *Journal of Composite Materials,* 34(05):420-441, 2000.

[14] Dharmawan F., Simpson G., Herszberg I. and John S. Mixed Mode Fracture Toughness of GFRP Composites. *Composites Structures*, 75:328-338, 2006.

[15] Ducept F., Gamby D. and Davis P. A Mixed-mode Failure Criterion Derived Tests on Symmetric and Asymmetric Specimens. *Composite Science and Technology*, 59:609-619, 1999.

[16] De Morais A. B. and Pereira A. B. Mixed Mode I + II Interlaminar Fracture of Glass/Epoxy Multidirectional Laminates –Part 1: Analysis. *Composite Science and Technology,* 66:1889-1895, 2006.

[17] ASTM D6671/D 6671M-06. Standard Test Method for Mixed Mode I-Mode II Interlaminar Fracture Toughness of Unidirectional Fiber Reinforced Polymer Matrix Composites. *ASTM International*, Philadelphia, PA, 2006.

[18] Sriram P., Khourchid Y., Hopper S.J. and Martin R.H. Experimental Development of a Mixed-Mode Fatigue Delamination Criterion. *Composite Materials: Fatigue and Fracture – Fifth Volume, ASTM STP 1230,* R.H. Martin Ed., ASTM International, Philadelphia, PA, 1995.

[19] Carlsson L.A., Matteson R.C., Aviles F. and Loup D.C. Crack Path in Foam Cored DCB Sandwich Fracture Specimens. *Composite Science and Technology*, 65:2612-2621, 2005.

[20] Kanninen M.F. An augmented Double Cantilever Beam Model for Studying Crack Propagation and Arrest. *International Journal of Fracture*, 9:83-91, 1973.

[21] Triantafillou T.C. and Gibson L.J. Debonding in Foam-Core Sandwich Panels. *Materials and Structures*, 22:64-69, 1989.

[22] Carlsson L.A. On the Design of the Cracked Sandwich Beam (CSB) Specimen. *Journal of Reinforced Plastic and Composites*, 10:434-444, 1991.

[23] Quispitupa A., Berggreen C. and Carlsson L.A. A debonded Sandwich Specimen under Mixed Mode Bending (MMB). *8th International Conference on Sandwich Structures ICSS 8*, Porto, May 3-6, 2008

[24] Hutchinson J.W. and Suo Z. Mixed Mode Cracking in Layered Materials. *Advances in Applied Mechanics*, J.W. Hutchinson and T.Y. Wu Eds. 29:63-191, 1992.

[25] Dundurs J. Effect of Elastic Constants on Stress in Composites under Plane Deformation. *Journal of Composite Materials*, 1(3):310-322, 1967.

[26] ANSYS 11, *User Manual*. Swanson Analysis System, Houston, PA.

[27] DIAB. *Technical Manual*. Divinycell H, Denmark, 2006.

[28] Viana G.M. and Carlsson L.A. Mechanical Properties and Fracture Characterization of Cross-Linked PVC Foams. *Journal of Sandwich Structures and Materials*, 4:99-113, 2002.

[29] Thouless M.D. Fracture of a Model Interface under Mixed-Mode Loading. *Acta Metall. Matter.*, 38(6):1135-1140, 1990.

[30] Berggreen C., Simonsen B.C. and Borum K.K. Experimental and Numerical Study of Interface Crack Propagation in Foam Cored Sandwich Beams. Journal of Composite Materials, 41(4):493-520, 2007.